An Optimal Sonar Array for Target Localization and Classification

Lindsay Kleeman
Intelligent Robotics Research Centre
Dept of Electrical & Computer Systems Eng.
Monash University, Australia

Roman Kuc
Intelligent Sensors Laboratory
Department of Electrical Engineering
Yale University, USA

Abstract

A novel sonar array for mobile robots is presented with applications to localization and mapping of indoor environments. The ultrasonic sensor localizes and classifies multiple targets in two dimensions to ranges of up to 8 meters. By accounting for effects of temperature and humidity, the system is accurate to within 1 mm and 0.1 degrees in still air. Targets separated by 10 mm can be discriminated. Targets are classified into planes, corners, edges and unknown, with the minimum of two transmitters and two receivers. A novel approach is that receivers are closely spaced to minimize the correspondence problem of associating echoes from multiple targets. A set of templates is generated for echoes to allow the optimal arrival time to be estimated, and overlapping echoes and disturbances to be rejected.

1. Introduction

Ultrasonic sensors provide a cheap and reliable means for robot localization and environmental sensing when the physical principles and limitations of their operation are well understood. A sensor design is presented that approaches the fundamental physical limitations of sonar in terms of accuracy and discrimination. The properties of air, reflectors and noise are the limiting factors.

We concentrate on environments composed of specular surfaces, such as smooth walls, bookcases, tables and chairs that reflect acoustic energy analogously to a mirror reflecting light. Rough surfaces can be treated with other techniques [1]. The applications of primary interest are robot localization from sensing known environmental features, such as wall and corner positions [2, 3, 4], and conversely, mapping of unknown environments for localization and navigation [5, 6, 7, 8]. Obstacle avoidance [9, 10] is another application of the sensor.

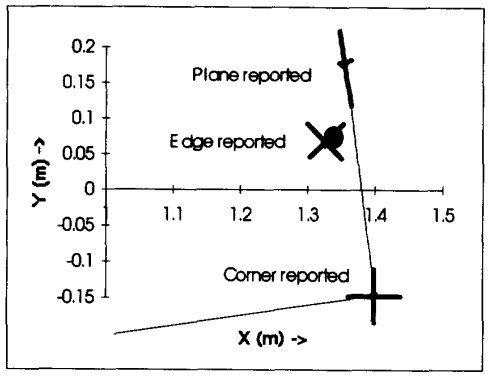

Figure 1 - Sensor reporting a 25 mm diameter table leg as an edge, and a corner and plane. The sensor is at the origin and points along the X-axis.

An emerging classification standard for two dimensional indoor target types is that of planes, corners and edges [2, 5, 11, 12, 13]. A *plane* is assumed to be a vertical smooth flat surface that reflects ultrasound specularly. A *corner* is a concave intersection of two planes at right angles, and an edge is assumed to reflect ultrasound from a point that is approximately independent of the transmitter and receiver positions.

The sensor approach presented here is novel in the sense that it classifies *all* three target types with the *one* stationary sensor, simultaneously in some cases, with high accuracy and discrimination. For example in Figure 1, the sensor views a table leg in front of a corner. In one measurement, the sensor localizes and classifies the corner, the table leg (as an edge) and a plane. Our approach has higher speed and accuracy, particularly in bearing, compared to single transducer systems that rely on multiple displaced readings and wheel odometery for

1050-4729/94 $03.00 © 1994 IEEE

target classification [1, 2]. Sonar sensors have been reported previously that can classify two of the three target types -- Barshan and Kuc [11] discriminate planes and corners based on pulse amplitude measurements; and Peremans *et al* [12] uses time of flight (**TOF**) to classify planes and edges and employs sensor movement to distinguish corners and planes. Three dimensional sonar target classification of planes and concave corners based on pulse amplitude measurements is proposed in [14]. Other sonar array sensors that report range and bearing to targets have been reported [13, 15, 16]. Space limits prevent a full treatment of our sensor design in this paper and the reader is referred to [17].

2. Sensor Configuration

The sensor arrangement employed in this paper is shown in Figure 2. There are two receivers and two transmitters which is the minimum required to identify planes, corners and edges of any orientation from stationary transducers [17]. Unlike other systems [12, 13], the receivers are *closely* spaced to minimize any correspondence ambiguity that may arise from multiple echoes arriving on both receivers. With the 35 mm spacing, targets must be separated by less than approximately 9 mm in range to cause a correspondence problem with an assumed transducer beam width of 60^{o} [17]. The two receiver transducers form a *vector sensor* from which bearing and range to targets can be estimated from the *distance of flights* (**DOF**) of a transmitter pulse. Due to the accurate DOF estimation technique employed, precise bearings can be still estimated with the closely spaced receivers. The transmitters are spaced sufficiently to perform reflector classification at the furthest range conceived for the sensor of 8 m. Polaroid 7000 series devices [18] are used in the sensor with their protective covers removed to eliminate reverberation, thereby producing shorter cleaner pulses.

The sensor arrangement has one less receiver than other published systems [12, 13] which employ three receivers in an attempt to resolve correspondence ambiguities. A receiver is a significant saving due to the data capture and processing requirements of a receiver channel. The deployment of a second transmitter in the sensor is comparatively cheap in terms of hardware, but does incur an additional measurement delay since transmitters need to be fired alternately.

Figure 2 - Sensor arrangement, T=transmitter R=receiver V=vector receiver.

The sensor array is interfaced to a 33 MHz 386 PC via a Biomation 8100 dual channel transient recorder with 8 bit conversion at a sample rate of 1 MHz as shown in Figure 3. The PC controls the firing of the transmitters and the triggering and control of the Biomation transient recorder. All processing and display of the received data are performed on the PC. The interface electronics consists of two simple receiver preamplifiers and two single transistor transmitter circuits. A 300V DC power supply provides the transducer biasing.

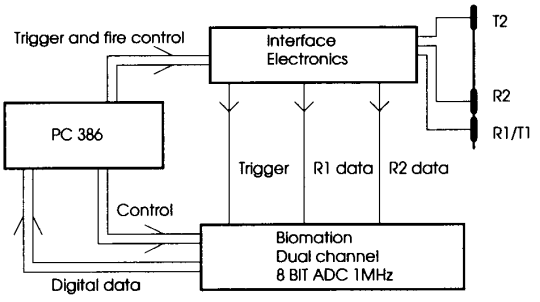

Figure 3 - Experimental Setup for Sensor.

2.1. Sensor Interaction with Target Types.

Figure 4 shows the sensor encountering a plane reflector. The vector receiver provides bearing estimates from both transmitters. The range, r_2, and bearing, α_2, of the virtual image T2' are functions of the range, r_1, and bearing, α_1, of the virtual image T1'. Consequently, we can write $r_{2plane}(r_1, \alpha_1)$ and $\alpha_{2plane}(r_1, \alpha_1)$. From triangle T1/V T2' A, the bearing difference between the two transmitters is

$$\beta_{plane} = \tan^{-1}\left(\frac{b\cos\alpha_1}{r_1 - b\sin\alpha_1}\right) \quad (1)$$

and

$$\alpha_{2plane}(\alpha_1, r_1) = \alpha_1 + \beta_{plane} \quad (2)$$

$$r_{2plane}(\alpha_1, r_1) = \sqrt{r_1^2 - 2r_1 b\sin\alpha_1 + b^2} \quad (3)$$

Note that the plane must be sufficiently wide to produce the two reflections. For $r_1 >> b$, the plane must be at least $(b\cos\alpha_1)/2$ wide.

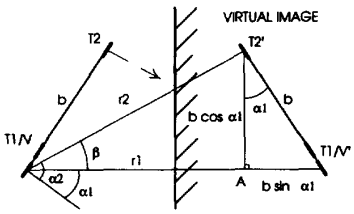

Figure 4 - Sensor image in a plane reflector.

The virtual image of the sensor in a corner is obtained by reflecting the sensor about one plane of the corner and then the other plane. This gives rise to a reflection through the point of intersection of the corner as shown in Figure 5. The situation is similar to the plane except that the angle between the transmitter images is opposite in sign: $\beta_{corner} = -\beta_{plane}$.

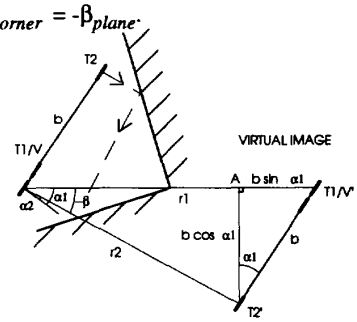

Figure 5 - Sensor image in corner reflector.

An edge represents physical objects such as convex corners and high curvature surfaces, where the point of reflection is approximately independent of transmitter and receiver positions. Consequently, the reflection from an edge has equal bearings from each transmitter ($\alpha_{2edge}(r_1, \alpha_1) = \alpha_1$). The DOF, r_{2edge} is given by

$$r_{2edge}(\alpha_1, r_1) = \frac{r_1 + \sqrt{r_1^2 + 4b^2 - 4r_1 b\sin\alpha_1}}{2} \quad (4)$$

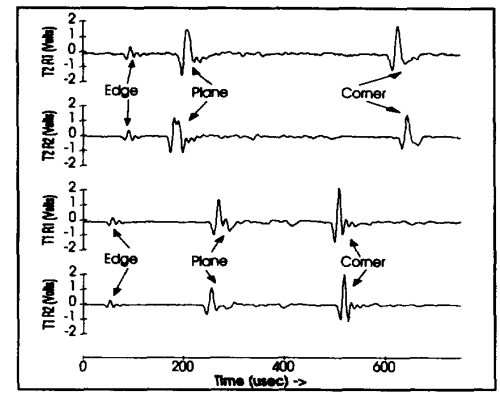

Figure 6 - Received echo data corresponding to Figure 1.

3. Target Classification

In this section we briefly describe the basis on which the sensor can discriminate between planes, corners and edges. A chi-squared statistic is derived in [17] for discriminating the target types to a specified level of confidence.

From the previous section, the differences between planes, corners and edges can be seen in terms of the sensor perception. The difference between echo bearings from the two transmitters is β_{plane} for a plane, $-\beta_{plane}$ for a corner and *0* for an edge and can be used to discriminate planes, corners and edges. The DOF information can be exploited to aid differentiation of edges from corners and planes. For small bearing angles and range much larger than the sensor baseline, b, $\beta_{plane} \approx b/r_1$. Also for the DOF r_2 the difference between a corner or plane and an edge is approximately $b^2/2r_1$. As ranges increase these margins decrease. On the other hand the standard deviations of errors in bearing and DOF increase, and a range limit for the sensor discrimination capability is reached at around 8 m in practice. For each of the target types, the received pulses are shown in Figure 6, corresponding to the targets in Figure 1. Note that in the bottom two traces, the pulses arrive at almost the same time for each target (bearings close to 0). In the top two traces (T2), the edge pulses

arrive at almost the same time ($\beta=0$), the plane R1 after R2 ($\beta>0$) and the corner R1 before R2 ($\beta<0$).

4. Modeling Pulse Shape

Estimating bearing and range to reflectors depends on an accurate TOF estimate. The maximum likelihood estimate of TOF of an echo pulse with additive Gaussian white noise is obtained by finding the maximum of the cross-correlation function of the received pulse with the known pulse shape [19]. Modeling the pulse shape is important for determining TOF and also for rejecting overlapping echoes and disturbances.

The pulse shape depends on many factors: transducers, excitation, angles to the transmitter and receivers, dispersion and absorption with distance of travel in air, and reflector properties. We assume a linear model for these effects. Let $s(t)$ be the sending excitation applied to the transmitter, then the signal recorded at the receiver is given by

$$rec(t,\theta_T,r_T,\theta_R,r_R) = s(t-\frac{r}{c}) * h_{trans}(t,\theta_T) * \frac{1}{\rho} h_{air}(t,r) * h_{refl}(t) * h_{rec}(t,\theta_R) \quad (5)$$

where * is the convolution operator and h's are impulse responses due to the transmitter at angle θ_T to axis, air absorption and dispersion, the reflector, and the receiver at angle θ_R to normal incidence. The distance r is defined as the total DOF r_T+r_R, where r_T is from the transmitter to the reflector and r_R from the reflector to the receiver. For plane and corner reflectors, ρ is defined to be the sum r_T+r_R, since a spherical wave front can be modeled as coming from a virtual transmitter at range r_T+r_R. For edge reflectors, ρ is defined as the *product* $r_T r_R$, since energy is effectively re-radiated from the point source located at the edge. The proportion of energy re-radiated from the edge is dependent on the area profile presented to the incoming wave front [20].

Since air is assumed to be a linear medium, the following property holds

$$h_{air}(t,r_1+r_2) = h_{air}(t,r_1) * h_{air}(t,r_2) \quad (6)$$

The transducers are much further from the reflector compared to their size, and therefore the impulse responses due to the transmitter and receiver can be further refined as [22] :

$$\begin{aligned} h_{trans}(t,\theta_T) &= h_\theta(t,\theta_T) * h_T(t) \\ h_{rec}(t,\theta_R) &= h_\theta(t,\theta_R) * h_R(t) \end{aligned} \quad (7)$$

where h_T and h_R are the impulse responses of the transmitter and receiver at normal angle of transmission and incidence. The angular impulse response, h_θ, is derived in [22]. From equations (6) and (7), equation (5) can be rewritten as:

$$rec(t,\theta_T,r_T,\theta_R,r_R) = ref(t-\frac{r}{c}) * h_\theta(t,\theta_T) * \frac{\rho_{ref}}{\rho} h_{air}(t,r-r_{ref}) * h_\theta(t,\theta_R) \quad (8)$$

where

$$ref(t) = s(t) * h_R(t) * \frac{1}{\rho_{ref}} h_{air}(t,r_{ref}) * h_{refl}(t) * h_R(t) \quad (9)$$

is obtained by storing a reference echo from a plane aligned to the transmitter and receiver at a range of 1 m as shown in Figure 7 where the corresponding beam pattern is also plotted. Note the absence of side lobes due to the wide bandwidth of the pulse shape.

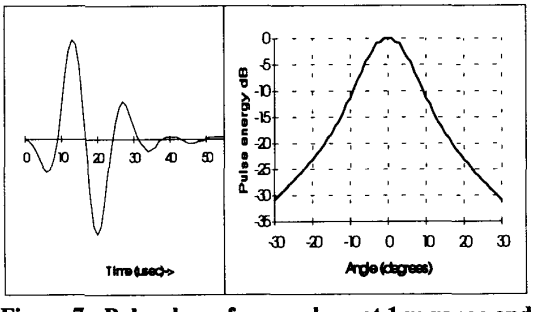

Figure 7 - Pulse shape from a plane at 1 m range and corresponding beam pattern.

The remaining function, h_{air}, is determined by calibration as described below. A matrix of templates of received pulse shapes is generated off-line for angles 0 to 20° in 1° steps and ranges 1 to 7 m in 1 m steps. The appropriate range can be selected from an approximate estimate of the arrival time, and the angles chosen from the best cross-correlation match.

4.1. Ultrasound Absorption and Dispersion

The air propagation medium absorbs sound energy as a function of temperature, humidity and frequency. Measured data [23] of absorption losses of still air at 20° C are plotted in Figure 8. The same data report the speed of sound from which the phase delay per meter can be shown to fit a minimum phase model for the absorption versus frequency [17]. The minimum phase is derived from the attenuation using the discrete Hilbert transform [21]. The inverse discrete Fourier transform is used to generate the impulse response for air at 20° C.

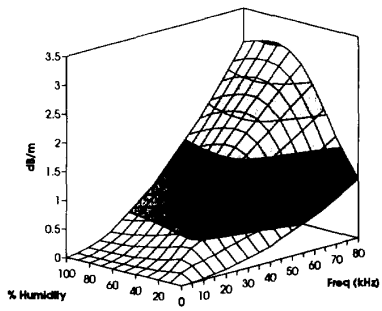

Figure 8 - Absorption loss (dB/m) in still air at 20° C - data derived from [23].

The absorption loss of air is a function of temperature and the data at 20° C is therefore not sufficient for estimating the impulse response. In practice it is only necessary to produce an impulse response function that *fits the observed data well.* Our approach is to use scaled versions of the 20° C data to account for variations in temperature. In addition to our reference pulse, *ref*, at 1 m, we collect another pulse, *ref2*, from a plane at a range of 3 m and minimize the square difference of the experimental *ref2* and the predicted pulse from the model. In order to test the model, predicted and experimental data are compared at ranges *different* to the 1 and 3 meters used for calibration. These are shown in Figure 9 at 2 meters and 5 meters range. The estimated impulse response of air thus performs well for both interpolation and extrapolation.

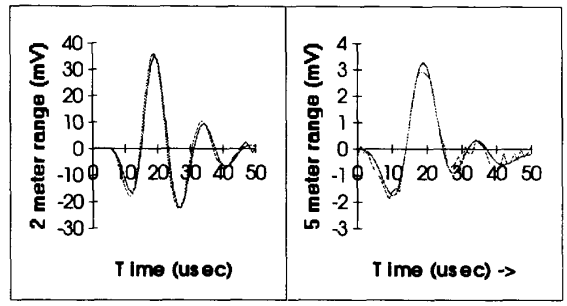

Figure 9 - Predicted (solid) and measured (dotted) pulses at 2 and 5 m ranges from an aligned plane.

5. Experimental Results for the Sensor

We positioned an acrylic plane at 200 mm increments from 2 meters up to 4 meters using a tape measure for range and the reflection of a laser off the plane for alignment. At each point, the mean and standard deviation of 100 sensor readings were recorded. The speed of sound was calibrated by using a straight line fit to the measurements. The maximum error was 0.8 mm which is comparable to our tape measuring accuracy. The standard deviations were all approximately 0.2 mm.

For bearing accuracy, we took measurements in a direction perpendicular to the sensor look direction. At a range of 4 meters we moved a corner in 200 mm increments to 1 meter off axis in both directions. The errors in bearing were less than 0.2° over a 20° range, with a typical standard deviation of 0.05°.

The sensor successfully classified planes and corners to a range of 7 m on axis. Edges were tested with cylinders of diameter 13 mm and 165 mm and were classified correctly to ranges of 2 and 3 m respectively.

To demonstrate the best discrimination achieved by the sensor, two 13 mm diameter cylinders 1 meter tall were positioned at a range of 750 mm with centres 30 mm apart and rotated until the sensor could only just discriminate the targets. The difference in range of the cylinders was 10 mm and difference in bearing was 1.9°. The limiting factors were the correspondence problem of associating the two echoes on each receiver and overlapping of the pulses. We reject arrival times when there is any possibility of ambiguity. This means

reflectors must be separated in range by at least 9 mm [17]. Echo overlap also becomes a limitation at range separations around 10 mm.

The software for the sensor was implemented in C on a PC 386 running at 33 MHz. Echo pulses are identified by looking for maxima above the noise floor and above neigbouring peaks within a pulse width. This means that the correlation processing is performed only on the actual candidates for the echo and not the entire signal. When all 21 template angles are correlated with each echo, the processing and sensing time is 1 second for one reflector. This includes graphic display and communications overhead to the data capture system. A faster approach and almost as accurate is to correlate with every second template angle until a local maximum occurs. This results in a three times speed up.

6. Conclusions

A novel sonar sensor configuration and processing approach has been presented that can accurately classify and localize planes, corners and edges without sensor movement. This has been achieved by adopting physical models for transmission, propagation, reflectance and reception of ultrasonic pulses combined with optimal arrival time processing, all with a reasonable computational burden. A template matching approach has been effective in optimally estimating the echo arrival times. The sensor range and bearing accuracy and target discrimination are often limited only by the fundamental properties of the transducer, air and reflectors, rather than the sensor data processing. A minimal sensor transducer configuration for classifying planes, corners and edges has been implemented.

References

[1] Bozma O and Kuc R, "Characterizing pulses reflected from rough surfaces using ultrasound", Journal Acoust. Soc. America, Vol 89, No 6, 1991, pp 2519-2531.

[2] Leonard J F and Durrant-Whyte H F, "Mobile robot localization by tracking geometric beacons", IEEE Journ. R&A Vol. 7 No 3, 1991 pp 376-382,

[3] Nagashima Y and Yuta S, "Ultrasonic sensing for a mobile robot to recognize an environment - measuring the normal direction of walls", Proc IROS 1992, pp. 805-812.

[4] Curran A and Kyriakopoulos K J, "Sensor-based self localization for wheeled mobile robots", IEEE Conf. R&A, Atlanta, May 1993, pp 8-13.

[5] Bozma O and Kuc R, "Building a sonar map in a specular environment using a single mobile sensor" IEEE PAMI Vol 13 No. 12 1991, pp. 1260-1269.

[6] Iijima J and Yuta S, "Searching unknown 2-D environment by a mobile robot with a range sensor", Computers Elect. Eng. Vol 18 No 1 1992 pp 83-98.

[7] Elfes A, "Sonar-based real world mapping and navigation", IEEE Journ. R&A, 1987, pp. 249-265.

[8] Crowley J L, "Navigation for an intelligent mobile robot", IEEE Journ. R&A, March 1985, pp. 31-41.

[9] Kuc R, "A spatial sampling criterion for sonar obstacle detection", IEEE Trans PAMI, Vol 12, July 1990, pp. 686-690.

[10] Borenstein J and Koren Y, "Obstacle avoidance with ultrasonic sensors", IEEE Journ. R&A, April 1988, pp 213-218.

[11] Barshan B and Kuc R, "Differentiating sonar reflections from corners and planes by employing an intelligent sensor", IEEE PAMI, Vol 12, No 6, 1990, pp 560-569.

[12] Peremans H, Audenaert K and Van Campenhout J M, "A high-resolution sensor based on tri-aural perception", IEEE Journ. R&A, Feb 1993, pp. 36-48.

[13] Sabatini A, "Active hearing for external imaging based on an ultrasonic transducer array", Proc IROS 1992, Raleigh, pp. 829-836.

[14] Hong M L and Kleeman L, "Analysis of ultrasonic differentiation of three dimensional corners, edges and planes", IEEE Conf. R&A, Nice, 1992 pp 580-584.

[15] Yang M, Hill S L, and Gray J O, "Design of ultrasonic linear array system for multi-object identification", Proc IROS 1992, Raleigh, pp. 1625-1632.

[16] Suoranta R, "Novel ultrasonic beamforming method based on nonlinear filtering", 1992 IEEE Ultrasonic Symposium, October 1992, Tucson, Arizona.

[17] Kleeman L and Kuc R, "Mobile robot sonar for target localization and classification", Technical report ISL-9301, Dept Elec. Eng., Yale University 1993.

[18] Polaroid Corporation, *Data sheet for Series 7000 transducer*, Ultrasonic components group, 119 Windsor St, Cambridge MA 02139 USA 1987.

[19] Woodward P M, *Probability and Information Theory with Applications to Radar*, Oxford, Pergamon Press 1964.

[20] Sasaki K and Takano M, "Classification of object's surface by acoustic transfer function", Proc IROS 1992, Raleigh, pp 821-828.

[21] Kuc R, *Introduction to Digital Signal Processing*, New York, McGraw-Hill 1988.

[22] Kuc R and Siegel M W, "Physical based simulation model for acoustic sensor robot navigation", IEEE PAMI, Vol 9, No 6, Nov 1987, pp 766-778.

[23] Weast R C and Astle M J, *CRC Handbook of Chemistry and Physics*, 59th ed, Boca Raton, CRC Press 1978.